INTERNATIONAL JOURNAL FOR NUMERICAL METHODS IN FLUIDS
Int. J. Numer. Meth. Fluids 2001; **36**: 35–52

High resolution flux-difference-splitting scheme on adaptive grid for open-channel flows

Akhilesh Kumar Jha*, Juichiro Akiyama and Masaru Ura

Department of Civil Engineering, Kyushu Institute of Technology, Sensui-cho, Tobata-ku, Kitakyushu-shi, Japan

SUMMARY

The effectiveness and usefulness of further enhancing the shock resolution of a second-order accurate scheme for open-channel flows by using an adaptive grid is investigated. The flux-difference-splitting (FDS) scheme based on the Lax–Wendroff numerical flux is implemented on a fixed as well as on a self-adjusting grid for this purpose. The grid-adjusting procedure, developed by Harten and Hyman, adjusts the grid by averaging the local characteristic velocities with respect to the signal amplitude in such a way that a shock always lies on a mesh point. This enables a scheme capable of perfectly resolving a stationary shock to capture a shock that moves from mesh point to mesh point. The Roe's approximate Jacobian is used for conservation and consistency, while theoretically sound treatment for satisfying entropy inequality conditions ensures physically realistic solutions. Details about inclusion of source terms, often left out of analyses for the homogeneous part of governing equations, are also explained. The numerical results for some exacting problems are compared with analytical as well as experimental results for examining improvements in resolution of discontinuities by the adaptive grid. Copyright © 2001 John Wiley & Sons, Ltd.

KEY WORDS: adaptive grid; approximate Riemann solver; conservative; flux-difference-splitting; numerical methods; unsteady flow

1. INTRODUCTION

Due to limitations of numerical concepts as well as computer capability, the early numerical methods for solving shallow water equations were simple, and in most cases a term by term translation of partial differential equations (PDEs) to finite difference equations [1]. It was soon realized that the numerical techniques must incorporate physical flow features and most importantly the directional property of signal propagation for greater accuracy and applicability [2,3]. However, these schemes failed to maintain conservative properties, which are particularly important in the case of discontinuous flows. Significant improvement in accuracy

* Correspondence to: Department of Civil Engineering, Kyushu Institute of Technology, Sensui-cho 1-1, Tobata-ku, Kitakyushu-shi 804-8550, Japan.

Received July 1999
Revised April 2000

has been reported by making the non-conservative Beam and Warming scheme fully conservative [4]. Recently, advances made in the field of gas dynamics in obtaining high resolution of discontinuous flows have shifted the focus of research from classical schemes to more sophisticated high-resolution, shock-capturing schemes for solving flow problems with strong discontinuities [5–7]. These schemes apply upwind differencing to a linearized Riemann problem. The higher-order versions of these schemes obtain oscillation-free results by employing flux or slope limiters.

Discontinuities present in a flow problem often pose serious difficulties for numerical treatment. The discontinuities may be due to the operation of control structures, such as sluice gates, a sudden change in channel geometry, such as bed slope, or a failure of hydraulic structures, such as a dam. Shock fitting and shock capturing have been the two most common approaches for resolving a shock while computing discontinuous flows. The shock-fitting approach isolates a bore and computes its propagation for one time step independently of the computation in the two adjacent continuous regions [8,9]. This approach, however, implies a prior knowledge of the occurrence of a shock. At the same time a shock must be tracked so that the Rankin–Hugoniot condition can be applied at the location of the shock. The problem is further compounded if there are many shocks appearing and disappearing as the solution proceeds in time.

These difficulties have given rise to the shock-capturing technique [10,11]. The shock-capturing technique does not treat a shock as a moving internal boundary, and the solution is obtained by integrating the governing equations in conservation form [12]. However, the shock-capturing technique might smear a shock when applied to a fixed-grid finite difference scheme. Extensions to a higher-order of accuracy do improve the shock resolution but cannot overcome problems inherent in the use of fixed-grid.

Another approach for avoiding the smearing of a shock is to track it and make its location coincide with a mesh point and then use a finite difference scheme capable of resolving a stationary shock. Although a shock has to be tracked in much the same way as in the case of shock-fitting approach, its treatment as a moving internal boundary is not required. Harten and Hyman [13] devised a self-adjusting grid that, when used with appropriate finite difference schemes, yields perfect shock resolution by ensuring that a shock always lies on a mesh point. Jha [14] implemented Roe's [15] first-order flux-difference-splitting (FDS) scheme on this self-adjusting grid and reported improved shock resolution for one-dimensional transient free surface flows.

In this paper, the effectiveness and usefulness of further enhancing shock resolution of a second-order accurate scheme for open-channel flows by using an adaptive grid is investigated. The second-order FDS scheme is developed using the Lax–Wendroff numerical flux and Roe's (1981) approximate Jacobian on a fixed grid as well as on the adaptive grid developed by Harten and Hyman [13]. Roe's [15] approximate Jacobian is made entropy-satisfying by suitable treatment [13]. The source term, often ignored as not-so-problematic when developing FDS schemes [6,7,14], has been identified as requiring equal attention [16]. Details for incorporating the source term are included in this paper. Numerical examples examining improvements in shock resolution due to the use of the self-adjusting grid, capabilities of the model to simulate complex channel flows and the effectiveness of the technique for handling source terms are also presented.

2. GOVERNING EQUATIONS

The governing equations for one-dimensional transient free surface flows are

$$\frac{\partial \mathbf{U}}{\partial t} + \frac{\partial \mathbf{E}}{\partial x} + \mathbf{S}_1 + \mathbf{S}_2 = 0 \tag{1}$$

where $\mathbf{U}$ is the vector of unknowns, $\mathbf{E}$ is flux vector and $\mathbf{S}_1$ and $\mathbf{S}_2$ are vectors containing source and sink terms respectively. These vectors for a prismatic channel of arbitrary cross-section are given as

$$\mathbf{U} = \begin{pmatrix} A \\ uA \end{pmatrix} \tag{‘2}$$

$$\mathbf{E} = \begin{pmatrix} uA \\ u^2A + gF_{\mathrm{h}} \end{pmatrix} \tag{3}$$

$$\mathbf{S}_1 = \begin{pmatrix} 0 \\ -gAS_0 \end{pmatrix} \tag{4}$$

$$\mathbf{S}_2 = \begin{pmatrix} 0 \\ -gAS_{\mathrm{f}} \end{pmatrix} \tag{5}$$

where A is the cross-sectional area of flow; u is the velocity; g is the acceleration due to gravity; S_0 is the bed slope and S_{f} is the friction slope given by the Manning's formula; F_{h} is the hydrostatic pressure force given by

$$F_{\mathrm{h}} = \int_0^h (h - \eta) W(\eta)\, \mathrm{d}\eta \tag{6}$$

where h is the flow depth; η is an integration variable indicating distance from channel bottom; and $W(\eta)$ is the channel width at η. The flux vector $\mathbf{E}$ is related to vector $\mathbf{U}$ through its Jacobian $\mathbf{J}$ as

$$\frac{\partial \mathbf{E}}{\partial x} = \mathbf{J} \frac{\partial \mathbf{U}}{\partial x} \tag{7}$$

and the Jacobian is given by

$$\mathbf{J} = \begin{bmatrix} 0 & 1 \\ gA/W(\eta) - u^2 & 2u \end{bmatrix} \tag{8}$$

The governing equations are hyperbolic, which implies that $\mathbf{J}$ has a complete set of independent and real eigenvectors. Therefore, $\mathbf{J}$ can be written in diagonalized form as

$$\mathbf{J} = \mathbf{e}\mathbf{D}_{\mathrm{m}}\mathbf{e}^{-1} \tag{9}$$

where $\mathbf{e}$ and $\mathbf{e}^{-1}$ are the matrix and inverse matrix of eigenvectors of $\mathbf{J}$ given by

$$\mathbf{e} = \begin{pmatrix} 1 & 1 \\ u + c & u - c \end{pmatrix} \tag{10}$$

$$\mathbf{e}^{-1} = \frac{1}{2c} \begin{pmatrix} -(u - c) & 1 \\ u + c & -1 \end{pmatrix} \tag{11}$$

where c is celerity expressed as

$$c = \sqrt{\frac{gA}{W(h)}} \tag{12}$$

and $\mathbf{D}_{\mathrm{m}}$ is the diagonal matrix of eigenvalues of $\mathbf{J}$ given by

$$\mathbf{D}_m = \begin{pmatrix} \lambda_1 & 0 \\ 0 & \lambda_2 \end{pmatrix} = \begin{pmatrix} u + c & 0 \\ 0 & u - c \end{pmatrix} \tag{13}$$

Roe [15] constructed an approximate Jacobian using the following average values of velocity and celerity:

$$\tilde{u} = \frac{A_{\mathrm{R}}^{1/2} u_{\mathrm{R}} + A_{\mathrm{L}}^{1/2} u_{\mathrm{L}}}{A_{\mathrm{R}}^{1/2} + A_{\mathrm{L}}^{1/2}} \tag{14}$$

$$\tilde{c}^2 = g \frac{\Delta(F_{\mathrm{h}})}{\Delta A} \tag{15}$$

where the operator is defined as

$$\Delta(\cdot) = (\cdot)_{\mathrm{R}} - (\cdot)_{\mathrm{L}} \tag{16}$$

and subscripts R and L refer to the left and right states. The approximate Jacobian can be used for the conservative evaluation of $\Delta\mathbf{E}$ by Equation (7). The approximate Jacobian satisfies the following properties:

$$\Delta \mathbf{U} = \tilde{\mathbf{e}}\tilde{\boldsymbol{\alpha}} \tag{17}$$

$$\Delta \mathbf{E} = \tilde{\mathbf{J}}\Delta \mathbf{U} = \tilde{\mathbf{e}}\tilde{\mathbf{D}}_{\mathrm{m}}\tilde{\boldsymbol{\alpha}} \tag{18}$$

From Equation (17), $\boldsymbol{\alpha}$, the column matrix of wave strengths, is obtained as

$$\tilde{\boldsymbol{\alpha}} = \tilde{\mathbf{e}}^{-1}\Delta \mathbf{U} = \begin{pmatrix} \Delta h/2 + (\Delta(uh) - \tilde{u}\Delta h)/2\tilde{c} \\ \Delta h/2 - (\Delta(uh) - \tilde{u}\Delta h)/2\tilde{c} \end{pmatrix} \tag{19}$$

3. SECOND-ORDER FDS SCHEME ON FIXED GRID

The second-order accurate Lax–Wendroff scheme for one-dimensional transient free surface flows can be written as

$$\mathbf{U}_i^{t+1} = \mathbf{U}_i^t - 0.5\gamma(\mathbf{E}_{i+1} - \mathbf{E}_{i-1}) + 0.5\gamma^2(\mathbf{J}_{i-1/2}(\mathbf{E}_{i+1} - \mathbf{E}_i) - \mathbf{J}_{i+1/2}(\mathbf{E}_i - \mathbf{E}_{i-1})) \tag{20}$$

where i and t are space and time indices respectively; $\gamma = \Delta t/\Delta x$, where Δt is the time increment and Δx is the finite difference grid size in space (Figure 1). All variables are at time level t if not indicated otherwise by superscripts. Equation (20) can also be written as

$$\mathbf{U}_i^{t+1} = \mathbf{U}_i^t - \gamma[\mathbf{F}_{i+1/2} - \mathbf{F}_{i-1/2}] \tag{21}$$

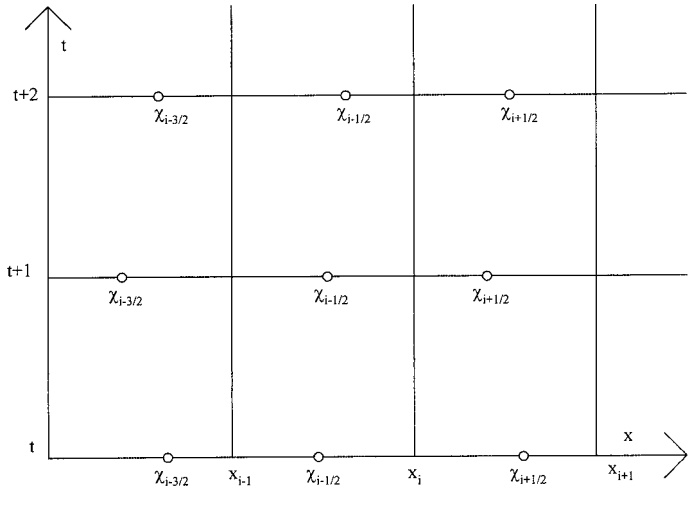

Figure 1. Variable grid and underlying fixed grid.

where **F**, called numerical flux, is given by

$$\mathbf{F}_{i+1/2} = \frac{1}{2}(\mathbf{E}_{i+1} + \mathbf{E}_i) - \frac{\gamma}{2}\mathbf{J}_{i+1/2}(\mathbf{E}_{i+1} - \mathbf{E}_i) \tag{22}$$

Using Roe's approximate Jacobian, Equation (22) can be written as

$$\mathbf{F}_{i+1/2} = \frac{1}{2}(\mathbf{E}_{i+1} + \mathbf{E}_i) - \frac{\gamma}{2}(\tilde{\mathbf{e}}\tilde{\mathbf{D}}_{\mathrm{m}}^2\tilde{\boldsymbol{\alpha}})_{i+1/2} \tag{23}$$

which can be mathematically manipulated to look like a first-order numerical flux with second-order terms added to it. This allows making the scheme total variation diminishing (TVD) by limiting the contribution of the second-order term by some flux limiter [17]. Therefore, the TVD numerical flux for Lax–Wendroff scheme can be written as

$$\mathbf{F}_{i+1/2} = \frac{1}{2}(\mathbf{E}_{i+1} + \mathbf{E}_i) - \frac{1}{2}(\tilde{\mathbf{e}}|\tilde{\mathbf{D}}_{\mathrm{m}}|\tilde{\boldsymbol{\alpha}})_{i+1/2} + \frac{1}{2}(\phi\,\tilde{\mathbf{e}}(|\tilde{\mathbf{D}}_{\mathrm{m}}| - \gamma\tilde{\mathbf{D}}_{\mathrm{m}}^2)\tilde{\boldsymbol{\alpha}})_{i+1/2} \tag{24}$$

The flux limiter ϕ is a non-linear function of

$$\mathbf{r}_{i+1/2} = (\boldsymbol{\alpha}_{i+1/2-\mathrm{sign}(\tilde{\lambda}_{i+1/2})}/\boldsymbol{\alpha}_{i+1/2}) \tag{25}$$

There are several types of non-linear functions of **r** available in the literature [17]. We used the Van Albada limiter in this study, which is expressed as

$$\boldsymbol{\phi} = (\mathbf{r} + \mathbf{r}^2)/(1 + \mathbf{r}^2) \tag{26}$$

The numerical scheme given by Equation (24) will be referred to as the Lax–Wendroff–Roe–Sweby (LWRS) scheme in the rest of this paper.

4. ENTROPY-SATISFYING TREATMENT

The approximate Jacobian computed using average velocity and celerity given by Equations (14) and (15) is conservative and consistent with the governing equations. However, it violates the entropy inequality condition, which results in the scheme converging to a non-physical solution in case of rarefaction waves. The problem can be remedied by replacing the modulus of $\mathbf{D}_{\mathrm{m}}$ in Equation (24) by a function $\mathbf{Q}_z$ defined as [13]

$$\mathbf{Q}_z = \begin{cases} |\mathbf{D}_{\mathrm{m}}|, & \text{if } |\mathbf{D}_{\mathrm{m}}| > \boldsymbol{\delta} \\ f(\mathbf{D}_{\mathrm{m}}, \boldsymbol{\delta}), & \text{otherwise} \end{cases} \tag{27}$$

The idea in the above treatment is to place an intermediate state between the left (L) and right (R) states. Depending on the definition of such an intermediate state, several alternatives can be devised for $f(\mathbf{D}_m, \boldsymbol{\delta})$. The following can be derived assuming continuous and linear averages for the intermediate state respectively:

$$f(\mathbf{D}_m, \boldsymbol{\delta}) = \boldsymbol{\delta} \tag{28}$$

and

$$f(\mathbf{D}_m, \boldsymbol{\delta}) = 0.5\left(\frac{\mathbf{D}_m^2}{\boldsymbol{\delta}} + \boldsymbol{\delta}\right) \tag{29}$$

$\boldsymbol{\delta}$ is a small positive quantity that can be either estimated by trial or computed by the following formula [13]:

$$\boldsymbol{\delta}_{i+1/2} = \max[0,\ \lambda(\mathbf{U}_i, \mathbf{U}_{i+1}) - \lambda(\mathbf{U}_i),\ \lambda(\mathbf{U}_{i+1}) - \lambda(\mathbf{U}_i, \mathbf{U}_{i+1})] \tag{30}$$

5. SOURCE TERM

Since $\mathbf{S}_2$ contains only friction terms and no derivative at all, it can be very well approximated by the Manning's formula. On the contrary, $\mathbf{S}_1$, although containing no derivative with respect to flow variables, contains derivatives with respect to the independent variable x. Roe [16] argued that, in linear systems, the source term $\mathbf{S}_1$ should be upwinded in the same way as the flux term $\mathbf{E}$. Applying the same idea in the present case, we can write

$$\mathbf{S}_1 = (\tilde{\mathbf{e}}\tilde{\mathbf{D}}_m\boldsymbol{\alpha}_s)/\Delta x \tag{31}$$

which yields

$$\tilde{\boldsymbol{\alpha}}_s = \frac{g\tilde{h}\Delta Z_b}{2\tilde{c}}\begin{pmatrix} 1/(\tilde{u}+\tilde{c}) \\ -1/(\tilde{u}-\tilde{c}) \end{pmatrix} \tag{32}$$

where Z_b is the bed elevation and the operator is given by Equation (16). To account for the source term, Equation (18) can be modified as

$$\Delta\mathbf{E} = \tilde{\mathbf{J}}\Delta\mathbf{U} = \tilde{\mathbf{e}}\tilde{\mathbf{D}}_m(\tilde{\boldsymbol{\alpha}} + \tilde{\boldsymbol{\alpha}}_s) \tag{33}$$

Consequently, the following terms must be added to the numerical flux (Equation (24)):

$$\mathbf{S}_{i+1/2} = -\frac{1}{2}(\tilde{\mathbf{e}}|\tilde{\mathbf{D}}_m|\tilde{\boldsymbol{\alpha}}_s)_{i+1/2} + \frac{1}{2}(\tilde{\mathbf{e}}\mathbf{D}_m\tilde{\boldsymbol{\alpha}}_s)_{i+1/2} \tag{34}$$

Finally, $\Delta t\mathbf{S}_2$ can be added to Equation (21).

6. ADAPTIVE GRID

The LWRS scheme on a fixed grid, as described in the preceding section, can perfectly resolve a shock if it lies at the extremities of the interval between $i+1/2$ and $i-1/2$. However, if a shock lies in the interior of this interval, which may often be the case, the shock is bound to be smeared. The maximum smearing would occur if a shock lies at the center of the interval between $i+1/2$ and $i-1/2$. A solution to this problem was suggested by Harten and Hyman [13] in the form of a variable grid that adjusts itself at each step of the computation. The adjustment is such that the location of a shock always coincides with a grid point, thereby resembling a stationary shock. The LWRS scheme on this self-adjusting grid yields resolution of a shock as a perfect discontinuity.

Details of the self-adjusting grid are referred to by Harten and Hyman [13] and Jha [14]. Only relevant equations are presented in the following. The self-adjusting grid and the underlying fixed grid are shown in Figure 1. The end-points of the variable grid are computed as

$$\tilde{\chi}^{t+1}_{i\pm 1/2} = X_{i\pm 1/2} + \left[\sum_{m=-1}^{1} (\bar{\chi}^{t+1}_{i+m\pm 1/2} - X_{i\pm 1/2})\beta_{i+m\pm 1/2} f(\bar{\chi}^{t+1}_{i+m\pm 1/2};\ x_i, x_{i\pm 1})\right] \Big/ \varphi_{i\pm 1/2} \tag{35}$$

where $X_{i\pm 1/2} = 0.5(x_i + x_{i\pm 1})$. The other terms in Equation (35) are computed as

$$\bar{\chi}^{t}_{i\pm 1/2} = \chi^{t}_{i\pm 1/2} + \Delta t v^{t}_{i\pm 1/2} \tag{36}$$

$$v_{i\pm 1/2} = \left\{\sum_{k=1}^{2} (\alpha^{k}_{i\pm 1/2})^2 \lambda^{k}_{i\pm 1/2}\right\} \Big/ \beta_{i\pm 1/2} \tag{37}$$

$$\beta_{i\pm 1/2} = \sum_{k=1}^{2} (\alpha^{k}_{i\pm 1/2})^2 \tag{38}$$

$$\varphi_{i+1/2} = \sum_{m=-1}^{1} \beta_{i+m+1/2} f(\chi_{i+m+1/2};\ x_i, x_{i+1}) \tag{39}$$

$$f(\chi_{i+m+1/2};\ x_i, x_{i+1}) = \begin{cases} 1, & x_i < \bar{\chi}_{i+m+1/2} \le x_{i+1} \\ 0, & \text{otherwise} \end{cases} \tag{40}$$

The computed interval end-points are finally modified by the following tests:

$$\chi_{i\pm 1/2}^{t+1} = \begin{cases} \tilde{\chi}_{i\pm 1/2}^{t+1}, & d_i^{t+1} > 0.5R_i \\ \tilde{\chi}_{i\pm 1/2}^{t+1} \pm 0.5R_i\varphi_{i\mp 1/2}/(\varphi_{i+1/2} + \varphi_{i-1/2}), & \text{otherwise} \end{cases} \tag{41}$$

where

$$d_i^{t+1} = \tilde{\chi}_{i+1/2}^{t+1} - \tilde{\chi}_{i-1/2}^{t+1} \tag{42}$$

At each step of the computation, new interval end-points are computed and the grid is automatically adjusted according to evolving solutions.

7. LWRS SCHEME ON A SELF-ADJUSTING GRID

The LWRS scheme on the aforementioned adaptive grid can be written as

$$\mathbf{U}_i^{t+1} = ((\Delta\chi)^t\mathbf{U}_i^t - \Delta t(\hat{\mathbf{F}}_{i+1/2} - \hat{\mathbf{F}}_{i-1/2}))/(\Delta\chi)^{t+1}, \quad \Delta\chi = \chi_{i+1/2} - \chi_{i-1/2} \tag{43}$$

where the numerical flux is expressed as

$$\hat{\mathbf{F}}_{i+1/2} = \frac{1}{2}(\hat{\mathbf{E}}_{i+1} + \hat{\mathbf{E}}_i) - \frac{1}{2}(\tilde{\mathbf{e}}|\hat{\tilde{\mathbf{D}}}_{\mathrm{m}}|\tilde{\boldsymbol{\alpha}})_{i+1/2} + \frac{1}{2}(\boldsymbol{\phi}\tilde{\mathbf{e}}(|\hat{\tilde{\mathbf{D}}}_{\mathrm{m}}| - \gamma\hat{\tilde{\mathbf{D}}}_{\mathrm{m}}^2)\tilde{\boldsymbol{\alpha}})_{i+1/2} \tag{44}$$

$$\hat{\mathbf{E}} = \mathbf{E} - v\mathbf{U} \tag{45}$$

$$(\hat{\tilde{\mathbf{D}}}_{\mathrm{m}})_{i\pm 1/2} = (\tilde{\mathbf{D}}_{\mathrm{m}})_{i\pm 1/2} - v_{i\pm 1/2} \tag{46}$$

8. NUMERICAL SIMULATIONS AND RESULTS

The examples are suitably designed to examine and demonstrate various aspects of this study. The first three examples are especially meant to examine improved shock resolution due to an adaptive grid. The channel conditions are idealized in these examples, which allow comparison of computed results with analytical solutions. The fourth example compares numerical results with experimental data. The fifth example demonstrates handling of the source term. The final example demonstrates the models' capability to compute flow over an almost-dry bed, wherein the numerical results are compared with the Ritter solution.

Equation (43) yields an integral solution of the problem which may be significantly different from the point-wise values at the finite difference nodes in the case of rarefaction waves. Consequently, plotting of these integral values as point-wise values may indicate the existence of several constant states, which is entirely a problem of a plotting algorithm. The problem can be avoided to some extent by a suitable averaging procedure [13]. However, we have ignored this aspect as it only affects the appearance of the plotted profile.

8.1. Sudden opening of sluice gate

The first example considers the sudden opening of a sluice gate in the middle of a 20-m long rectangular, horizontal and frictionless channel. The sluice gate is placed at mid-length of the channel. The gate retains 10-m deep still water to its left side while the remaining half of the channel has 0.05-m deep still water. The discontinuity in depth at the gate is specified as the initial condition that simulates the hydraulic condition resulting from the sudden opening of the sluice gate. Both upstream and downstream boundaries are kept closed. The computations are done with a fixed-grid size of 0.10 m.

The computed depth and velocity profiles soon after 0.2 s are shown in Figures 2 and 3 respectively. The analytical solutions are also plotted therein. A noticeable improvement in the shock resolution is seen as a result of using the LWRS scheme on the varying grid. The depth and velocity computed by both fixed and varying grid versions of the LWRS scheme agree perfectly well with the analytical solutions.

8.2. Sudden closure of sluice gate

This example considers the flow resulting from the sudden closure of a sluice gate in the channel of the previous example. Initially the sluice gate is fully open and the channel has 0.064-m deep water flowing at 1.82 $m\,s^{-1}$ (Froude number = 2.30). At supercritical inflow

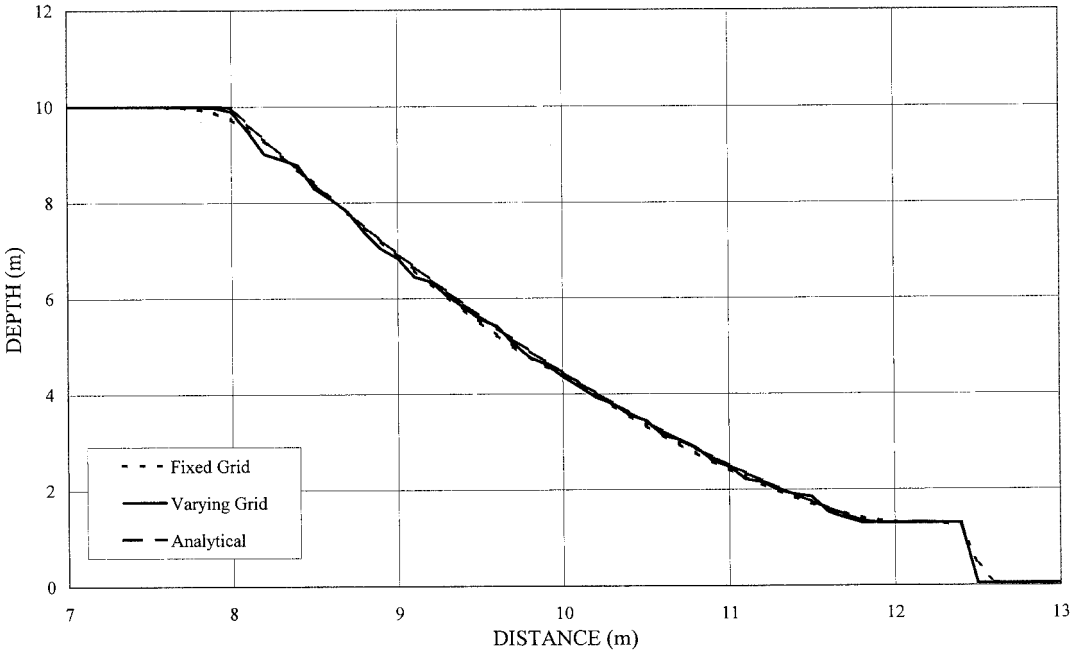

Figure 2. Depth profile 0.20 s after sudden opening of sluice gate.

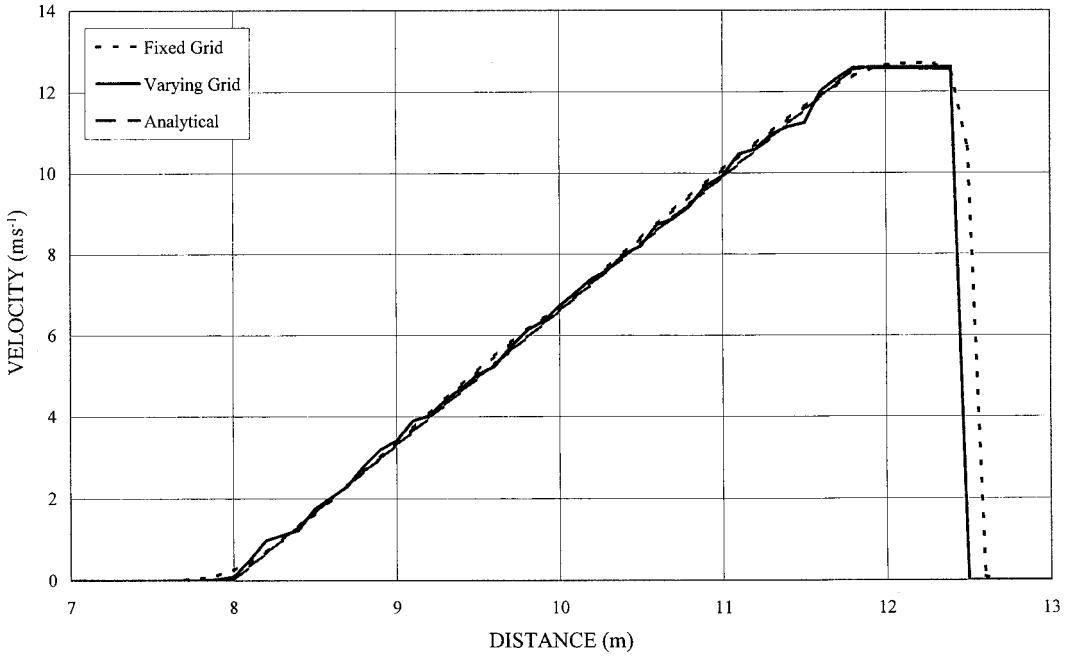

Figure 3. Velocity profile 0.20 s after sudden opening of sluice gate.

upstream, both depth and velocity are specified while no boundary condition is required at the supercritical outflow downstream. The fixed grid size is 0.10 m. At time 0.05 s the sluice gate is instantaneously closed. Upstream of the sluice gate, a reflected bore is formed, which travels upstream, leaving still water behind. Downstream of the sluice gate, a negative wave is formed whose profile stretches and recedes in the downward direction.

The computed results soon after 3.0 s are shown in Figure 4 along with the analytical solution. The bore upstream, as well as the negative wave downstream, are very well simulated by models on fixed as well as varying grids. The effect of the varying grid in terms of enhanced shock resolution is less obvious in this case than in the previous example.

8.3. Bore propagation and reflection

Propagation of a bore on still water and its reflection from the closed end is simulated in this example. The 40-m long rectangular channel is assumed to be horizontal and frictionless. The fixed grid size is 0.20 m. The initial condition in the channel is specified as 1-m deep still water throughout the channel. The downstream end is kept closed while at the upstream end a constant discharge of 50 $m^3 s^{-1}$ is maintained from the start of computation. The resulting bore travels downstream and eventually hits the downstream closed end. Thereafter, a reflected bore is formed that travels upstream.

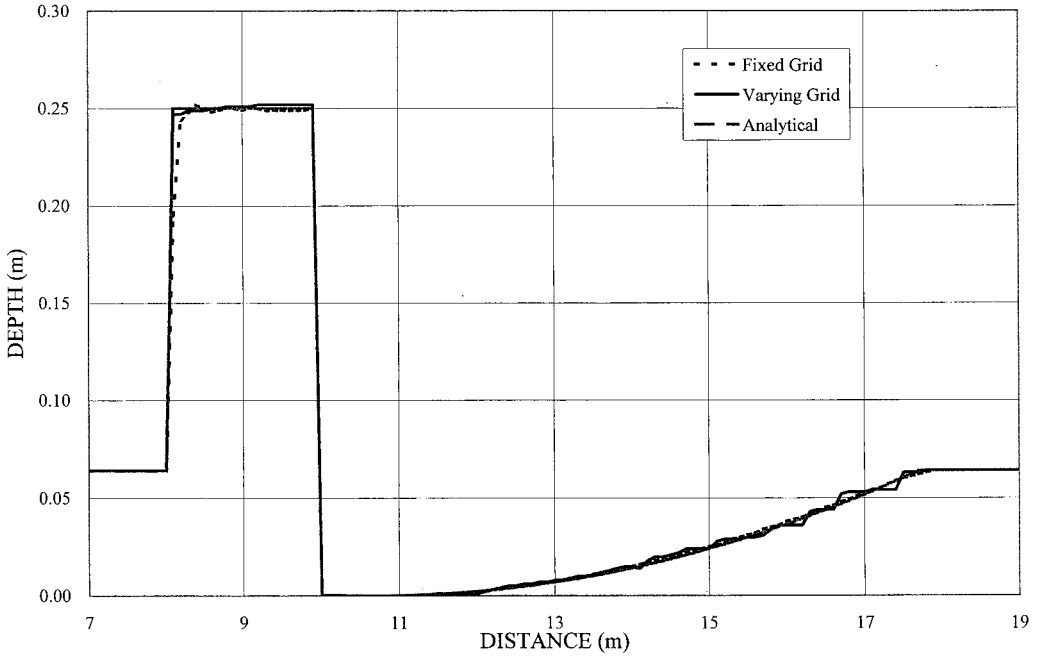

Figure 4. Depth profile 2.95 s after sudden closure of sluice gate.

Figure 5 shows the computed bore at 2 s and the reflected bore at 4 s. Analytical solutions are also plotted in the figure. It is evident that the models correctly compute the bore propagation and reflection. As expected, the use of the varying grid yields better shock resolution in this case.

8.4. Hydraulic jump in a channel

The next problem considers a hydraulic jump in a channel. This example is taken from experiments conducted by Gharangik [18] in a 13.9-m long and 0.45-m wide straight, horizontal rectangular channel with Manning's values of between 0.008 and 0.011. The constant discharge was 0.053 $m^3 s^{-1}$. The upstream flow depth was 0.064 m (velocity = 1.82 $m s^{-1}$, Foude number = 2.3) and the conjugate depth was 0.17 m (velocity = 0.69 $m s^{-1}$, Froude number = 0.53). The grid size for this problem is 0.05 m. At the upstream end, both depth and velocity are specified as required for supercritical inflow. The downstream end is provided with an overflow weir that is designed to maintain the required depth for the formation of a hydraulic jump. The weir across the channel width has crest at 0.048 m. We obtained good results with a Manning value = 0.009.

The steady state results are compared with experimental data in Figure 6. The location of jump at about 1.8 m agrees well with the experimental data and so does the jump height. It

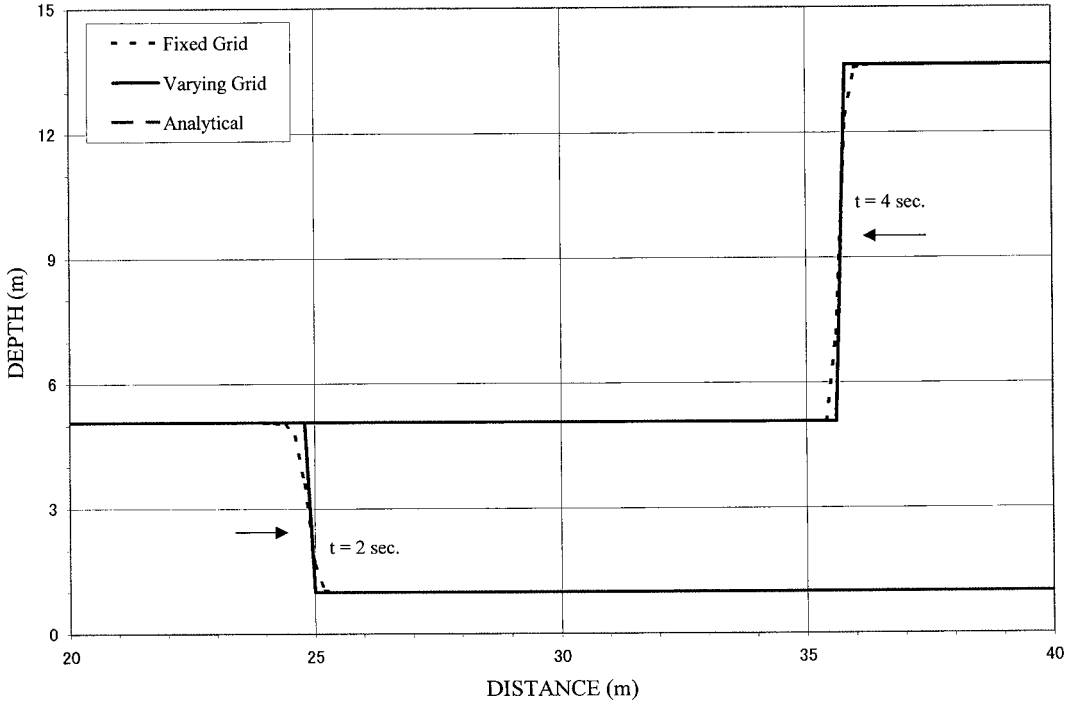

Figure 5. Bore propagation and reflection in a channel.

may be noted, however, that the shallow-water equations yield sharp discontinuities and therefore fail to correctly predict the length of the jump. There is no noticeable difference between results by fixed and varying-grid formulations. It may also be noted that the downstream weir is very well simulated by the models.

8.5. Reflected bore in sloping trapezoidal channel

This problem examines whether the source term is properly computed by the models. The example is taken from Fennema and Chaudhry [19]. The 5000-m long trapezoidal channel with a side slope of 1.5V:1.0H, longitudinal slope 0.0000785 and Manning's $n = 0.013$ constantly carries a uniform flow with velocity 1.47 $\mathrm{m\,s^{-1}}$ and depth 5.79 m. After the start of the computation, the flow velocity at the downstream end is reduced to zero, which leads to the formation of a shock that travels upstream. The fixed grid size is 10 m.

The computed results are shown in Figure 7 along with the results obtained by the Euler explicit version of the conservative Beam and Warming scheme [4]. While the problem is very well simulated, the difference in shock resolution between the varying grid and the fixed grid is not significant.

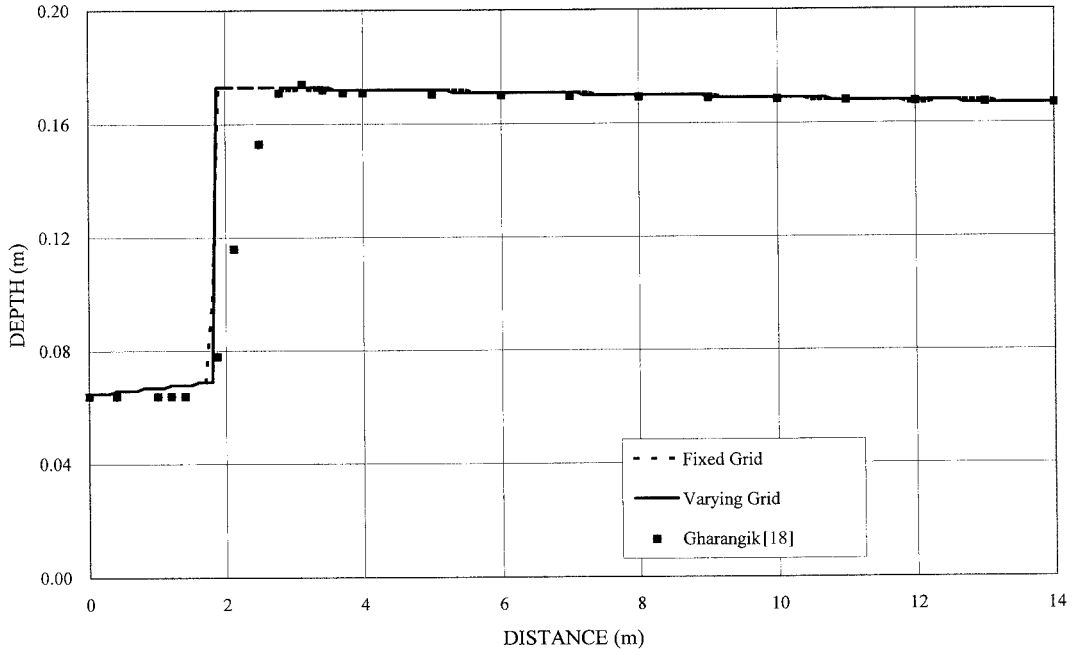

Figure 6. Computation of hydraulic jump and comparison with experimental data.

8.6. Flood-wave on dry bed

The propagation of a flood-wave on a dry bed is simulated in this example. The flood-wave results from a sudden collapse of a dam in the middle of a 40-m long rectangular, horizontal and frictionless channel. The fixed grid size is 0.20 m. The initial condition in the reservoir is 1.0-m deep still water. The LWRS scheme does not work below a tail-water depth-to-reservoir depth ratio of 0.005 and therefore Roe's first-order accurate scheme was used until the LWRS scheme became applicable [7]. An absolute zero depth in the tail-water causes mathematical problems. To avoid this, a negligible depth of 0.00001 m is assumed to exist initially below the dam.

The results at $3 + \Delta t$ s are shown in Figure 8 along with the Ritter solution. It is noted that the computed wave front lags slightly behind that of the Ritter solution. However, for most practical purposes, the computed results can be termed as reasonably good.

9. CONCLUSIONS

The second-order accurate FDS scheme based on the Lax–Wendroff numerical flux for simulating one-dimensional transient free surface flows is implemented on a self-adjusting grid

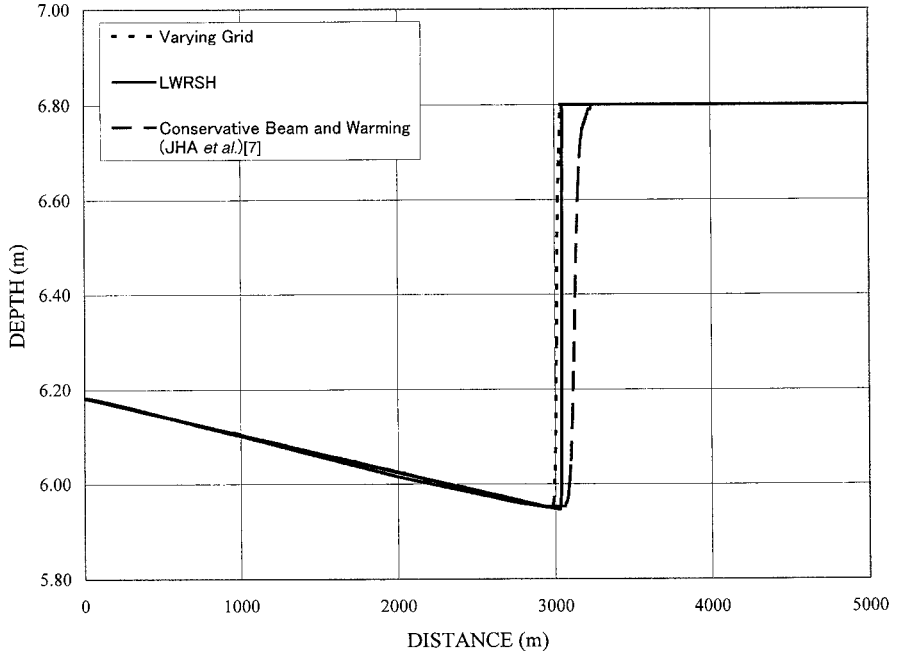

Figure 7. Reflected bore in a sloping, trapezoidal channel.

for examining improvement in shock resolution. The use of Roe's approximate Jacobian makes the scheme conservative and consistent with the governing equations. The source term has been treated in a way consistent with the general formulation of the FDS scheme. The model is applied to several specially designed problems and the results are compared with analytical solutions and with experimental data.

It is concluded that the LWRS scheme yields very good results for all the problems considered. The shock resolution does improve as a result of using the varying grid. However, the improvement is not found to be significant. This may be due to the fact that the shock resolution by the LWRS scheme on a fixed-grid itself is very good. The inclusion of source terms also complicates the matter for the adaptive grid because the adaptive grid developed by Harten and Hyman [13] is meant for a conservative scheme and inclusion of source terms introduces non-conservativeness. For very strong source terms, the LWRS scheme on an adaptive grid becomes increasingly unstable. In view of these limitations in using the adaptive grid and only marginal improvement in shock resolution, it is concluded that the use of an adaptive grid can only be justified for a specific problem requiring particularly high shock resolution.

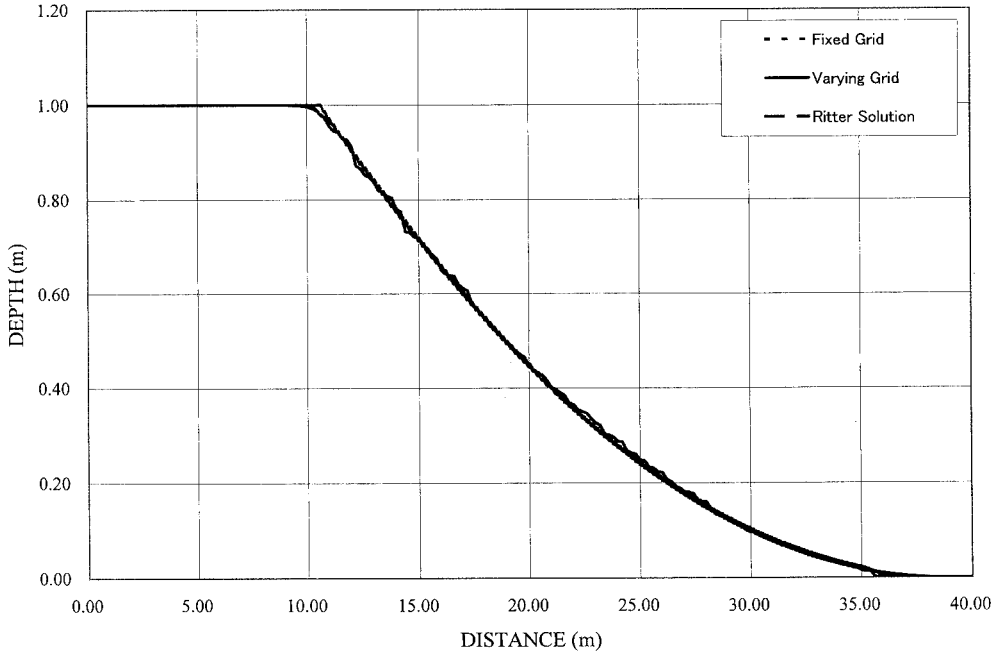

Figure 8. Flood-wave propagation on dry bed.

APPENDIX A. NOMENCLATURE

A	cross-sectional area of flow
c	celerity
d	grid size on self-adjusting grid
$\mathbf{D}_m$	diagonal matrix of eigenvalues of **J**
e	matrix of eigenvectors
E	flux matrix on fixed grid
$\hat{\mathbf{E}}$	flux matrix on self-adjusting grid
f	function of χ
F_h	hydrostatic pressure force term
F	numerical flux on fixed grid
$\hat{\mathbf{F}}$	numerical flux on self-adjusting grid
g	acceleration due to gravity
h	flow depth
i	grid location in space
J	Jacobian of **E** with respect to **U**
k	wave number

R	minimum of two adjacent intervals on fixed grid
S_0	bed slope
S_f	friction slope
$\mathbf{S}_1, \mathbf{S}_2$	matrix of source and sink terms
t	index for time
u	velocity
$\mathbf{U}$	vector for flow variables
v	speed of single discontinuity
$W(\eta)$	channel width at distance η from channel bottom
x	distance along channel

Greek letters

$\boldsymbol{\alpha}$	wave strength
$\boldsymbol{\alpha}_s$	wave strength equivalent for source term
β	sum of square of α
$\chi, \tilde{\chi}$	interval end-points on self-adjusting grid
$\bar{\chi}$	first guess value of interval end-points on self-adjusting grid
δ	small positive quantity
φ	weighted amplitude of the waves
γ	$\Delta t/\Delta x$
η	integration variable indicating distance from channel bottom
λ	eigenvalues of $\mathbf{J}$
$\tilde{\lambda}$	eigenvalues of $\mathbf{J}$ for Roe's scheme on self-adjusting grid
Δ	operator, i.e. $\Delta f_{i+1/2} = f_{+1} - f_i$

REFERENCES

1. Mahmood K, Yevjevich V (eds). *Unsteady Flow in Open Channels*. Water Resources Publications: Fort Collins, CO, 1975.
2. Gabutti B. On two upwind finite-difference schemes for hyperbolic equations in non-conservation form. *Computers and Fluids* 1983; **11**(3): 207–230.
3. Beam WM, Warming RF. An implicit finite-difference algorithm for hyperbolic systems in conservation-law form. *Journal of Computational Physics* 1976; **22**: 87–110.
4. Jha AK, Akiyama J, Ura M. A fully conservative beam and warming scheme for transient open channel flows. *Journal of Hydraulic Research* 1996; **34**(5): 605–621.
5. Glaister P. Approximate Riemann solution of the shallow water equations. *Journal of Hydraulic Research* 1988; **26**(3): 293–306.
6. Alcrudo F, Garcia-Navarro P, Saviron JM. Flux difference splitting for 1D open channel flow equations. *International Journal for Numerical Methods in Fluids* 1992; **14**: 1009–1018.
7. Jha AK, Akiyama J, Ura M. First and second-order flux difference splitting schemes for dam-break problem. *Journal of Hydraulic Engineering*, *ASCE* 1995; **121**(12): 877–884.
8. Katopodes ND, Strelkoff T. Computing two-dimensional dam-break flood waves. *Journal of Hydraulic Division*, *ASCE* 1978; **104**(HY9): 1269–1288.
9. Chen CL, Armbruster JT. Dam-break wave model: formulation and verification. *Journal of Hydraulic Division*, *ASCE* 1980; **106**(HY5): 747–767.
10. Lax PD. Weak solutions of non-linear hyperbolic equations and their numerical applications. *Communication on Pure and Applied Mathematics* 1954; **7**: 159–193.

11. Lax PD, Wendroff B. Systems of conservation laws. *Communications on Pure and Applied Mathematics* 1960; **13**: 217–237.
12. MacCormack RW. Numerical solution of the interaction of a shock wave with a laminar boundary layer. In *Lecture Notes in Physics*, vol. 8. Springer: New York, 1971; 151–163.
13. Harten A, Hyman JM. Self-adjusting grid method for one-dimensional hyperbolic conservation laws. *Journal of Computational Physics* 1983; **50**: 235–269.
14. Jha AK. Flux difference splitting on self-adjusting grid for 1-D transient free surface flows. *Journal of Hydroscience and Hydraulic Engineering JSCE* 1995; **13**(2): 43–54.
15. Roe PL. Approximate Riemann solvers, parameter vectors and difference schemes. *Journal of Computational Physics* 1981; **43**: 357–372.
16. Roe PL. Upwind differencing schemes for hyperbolic conservation laws with source terms. In *1st International Congress on Hyperbolic Problems*, *St. Etienne*, Carasso, Raviart, Serre (eds). Springer: Heidelberg, 1986; 41–51.
17. Sweby PK. High resolution schemes using flux limiters for hyperbolic conservation laws. *SIAM Journal of Numerical Analysis* 1984; **21**: 995–1101.
18. Gharangik AM. Numerical simulation of hydraulic jump. MSs thesis, Washington State University, WA, USA, 1988.
19. Fennema RJ, Chaudhry MH. Explicit numerical schemes for unsteady free surface flows with shocks. *Water Resources Research* 1986; **22**(13): 1923–1930.

